Hierarchically Structured One-Dimensional TiO_2 for Protein Immobilization, Direct Electrochemistry, and Mediator-Free Glucose Sensing

Peng Si,[†] Shujiang Ding,[†] Jun Yuan, Xiong Wen (David) Lou,[*] and Dong-Hwan Kim[*]

School of Chemical and Biomedical Engineering, Nanyang Technological University, 70 Nanyang Drive, Singapore 637457 [†]These authors contributed equally.

ABSTRACT A novel one-dimensional hierarchically structured TiO_2 (1DHS TiO_2) was synthesized by a solvothermal method using multiwalled carbon nanotubes (MWCNTs) as a template and evaluated for the immobilization of protein and biosensing applications. Characterization studies showed that the 1DHS TiO_2 possessed an anatase crystalline structure and a large surface area with narrow pore size distribution. Fast direct electron transfer was observed for glucose oxidase (GOx) immobilized on the 1DHS TiO_2, and excellent electrocatalytic performance for glucose detection can be obtained without a mediator. The glucose sensor based on the GOx/1DHS TiO_2-modified electrode had a high sensitivity of 9.90 μA mM^{-1} cm^{-2} and a low detection limit of 1.29 μM. The fabricated biosensor displayed good selectivity and long-term stability, indicating that the novel structured TiO_2 is a promising material for the immobilization of biomolecules and the fabrication of third-generation biosensors.

KEYWORDS: hierarchical TiO_2 · solvothermal synthesis · direct electrochemistry · glucose oxidase · biosensor

Promoting direct electron transfer (DET) between an electrode and immobilized molecules is of scientific importance in the investigation of the fundamental mechanism of biological redox reactions[1−3] and of practical significance for the development of advanced bioelectronic devices, such as highly sensitive enzymatic biosensors[4−6] and highly efficient biofuel cells.[7−9] However, the DET of proteins is rarely observed on bare electrodes because the redox center of the enzyme is deeply embedded in a thick insulating protein shell and the spacing between the prosthetic group and the electrode surface generally exceeds the critical electron-tunneling distance.[10,11] To facilitate the electron transfer, redox mediators (small diffusive molecules shuttling between the active center of the protein and the electrode surface) have been traditionally employed in the solution phase or immobilized on electrodes.[12−14]

Over the past decades, the exploration of nanomaterials designed to have high conductivity, good biocompatibility, suitable hydrophilicity, a large surface area, and a uniform porosity has fueled research on the impregnation of biomolecules and the construction of biosensors.[15−18] Nanomaterials with tailored textures appear to facilitate electron transfer between the electrode and immobilized proteins because the unique chemical, physical, and electrical properties of nanostructured materials may effectively shorten the electron-tunneling distance and provide an electron-mediating function.[19−22] Varied nanomaterials composed of carbon,[5,23,24] metal oxides,[25−27] and conducting polymers[28,29] have demonstrated the capabilities of DET. However, significant challenges remain in the development of a nanomaterial that shows fast electron transfer, precise specificity, high sensitivity, and superior bioelectrocatalysis. Due to its superior photocatalytic capability and excellent electron-transfer behavior, TiO_2 has been extensively investigated for use in a broad range of applications, including dye-sensitized solar cells,[30,31] hydrolysis catalysts,[32,33] electrochromic devices,[34,35] and lithium-ion batteries.[36,37] Nanocrystalline TiO_2 films have recently been introduced to improve the catalytic activity of enzymes in the applications of gas sensors[38−40] and biosensors.[41−43] The electrochemical properties of TiO_2-based devices are not only influenced by the crystalline form of the TiO_2 but also likely affected by the textural properties of the TiO_2 such as dimension, geometry, porosity, and surface area.[25,44] In addition, the quantum confinement effect and electron transport properties are largely governed by the size and geometry of nanostructured TiO_2.[45,46]

* E-mail: xwlou@ntu.edu.sg, dhkim@ntu.edu.sg.

Received for review July 19, 2011 and accepted August 25, 2011.

Published online August 25, 2011
10.1021/nn202714c

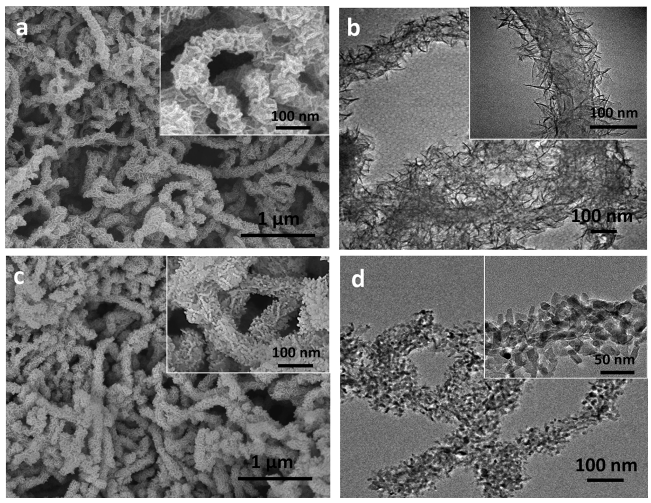

Figure 1. SEM (a, c) and TEM (b, d) images of the CNT-TiO_2 composite (a, b) and the 1DHS TiO_2 (c, d) obtained after calcining the composite at 550 °C for 2 h. Insets are the high-magnification SEM and TEM images.

A high surface area and a uniform pore distribution are especially beneficial for TiO_2-based bioelectronic devices because these properties promote the interaction between biomolecules and materials and allow for high accessibility of target molecules to the device surface. This high accessibility facilitates the reaction occurring at the medium/electrode interface.[44]

Template-assisted preparation methods have been used widely in nanoengineering due to their simplicity, cost-effectiveness, and shape-control capabilities during synthesis. A variety of templates, including porous anodic alumina,[47,48] polystyrene spheres,[49,50] surfactants,[51] and activated carbon,[52] have been employed to synthesize nanostructured materials with different morphologies, such as highly ordered nanowires,[53,54] nanotube arrays,[55,56] micro/nano hollow structures,[57,58] and mesoporous structures.[59−62] In the present work, a hierarchically structured one-dimensional TiO_2 was, for the first time, synthesized by a solvothermal method using multiwalled carbon nanotubes (MWCNTs) as a template. The synthesized material was characterized to be highly porous with a large surface area and a narrow distribution of pore sizes. The synthesized TiO_2 showed great biocompatibility for biomolecule immobilization and allowed direct electrochemical reactions for the anchored redox protein. In addition, the glucose-sensing abilities of the electrodes modified with the synthesized TiO_2 were determined in the absence of mediators.

RESULTS AND DISCUSSION

Material Characterizations. The surface morphology and microstructure of the synthesized TiO_2 were characterized by field emission scanning electron microscopy (FESEM) and transmission electron microscopy (TEM) (Figure 1 and Figure S1, Supporting Information). Figure 1a shows the scanning electron microscopy (SEM) image of the as-prepared CNT-TiO_2 nanocomposite synthesized *via* the solvothermal method. The composite displays an one-dimensional, rough, and porous structure with diameter of around 100 nm. The magnified SEM image (inset of Figure 1a) reveals a hierarchically structured surface morphology of the composite material. The TEM image in Figure 1b shows that carbon nanotubes (CNTs) in the composite are homogeneously encapsulated by TiO_2 nanoclusters that consist of ultrathin nanosheet-like structures (inset of Figure 1b). The formation of TiO_2 nanosheets on the CNT surface could be mainly attributed to the dual function of diethylenetriamine (DETA): catalyzing the hydrolysis of titanium(IV) isopropoxide (TIP) to form TiO_2 nanosheets[36] and assisting the self-assembly of the formed TiO_2 nanostructures on the surface of acid-treated CNT, possibly through electrostatic interactions.[37] Figure 1c shows the SEM image of TiO_2 obtained after calcining the CNT-TiO_2 composite at 550 °C for 2 h. The calcined TiO_2 maintains its one-dimensional (1D) structure after removing the CNT templates and displays more delicate surface textures (inset of Figure 1c). The TEM image of calcined TiO_2 (Figure 1d) reveals that the 1D TiO_2 has a hierarchical structure from which the CNT template has been completely removed. The diameter of the 1D hierarchically structured TiO_2 (1DHS TiO_2) is approximately 60−80 nm, much smaller than the CNT-TiO_2 composite, possibly because of the partial collapse of the hollowed TiO_2 structure during the annealing process.

The phase features of the synthesized TiO_2 were investigated by X-ray powder diffraction (XRD, Figure 2a). The pristine, uncalcined CNT-TiO_2 composite shows weak peak intensities (Figure 2a, pattern I), suggesting poor crystallinity of the uncalcined CNT-TiO_2. The two main peaks at 25 and 48° correspond to the anatase (101) and (200) diffraction, respectively (JCPDS) card no: 21-1272), indicating that anatase TiO_2 formed on the surface of CNT during the solvothermal treatment. The intensities of the XRD peaks are significantly enhanced after sintering the composite at 550 °C for 2 h (Figure 2a,

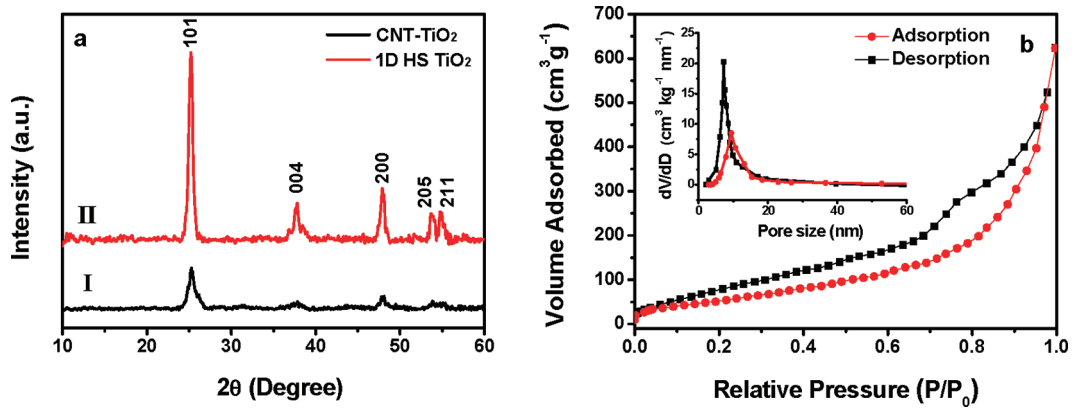

Figure 2. (a) XRD patterns for (I) the CNT-TiO_2 composite and (II) the 1DHS TiO_2 formed after calcination. (b) Nitrogen adsorption–desorption isotherms of the 1DHS TiO_2. Inset: Pore size distribution calculated from the adsorption branch and desorption branch of the isotherm by the Barrett–Joyner–Halenda method.

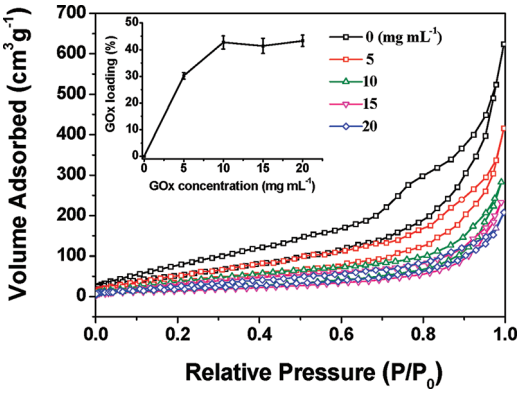

Figure 3. The nitrogen adsorption–desorption isotherms of 1DHS TiO_2 before and after loading with different GOx concentrations ranging from 0 to 20 mg mL^{-1}. Inset: The plot of the GOx loading ratio on 1DHS TiO_2 *versus* the GOx concentration.

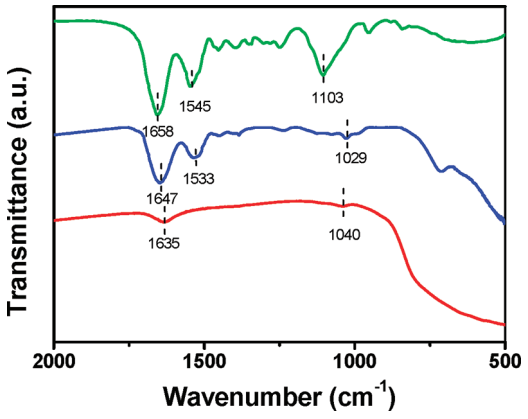

Figure 4. IR spectra of 1DHS TiO_2 (red), pure GOx (green), and GOx-loaded TiO_2 (blue).

pattern II), reflecting the high crystallinity and high purity of the resultant TiO_2 material. The identified peaks match perfectly with those of the standard XRD pattern of anatase TiO_2, with lattice constants of $a_0 = 3.785$ Å and $c_0 = 9.513$ Å, respectively. The chemical composition of 1DHS TiO_2 is investigated by energy dispersive X-ray spectroscopy (EDX), showing strong Ti and O signals (Figure S2, Supporting Infomation), which confirms the phase purity of the product.

The nitrogen adsorption–desorption isotherm (Figure 2b) of the 1DHS TiO_2 shows a type-H3 hysteresis loop with an abrupt increase in the adsorption branch at a high relative pressure (P/P_0), implying the presence of mesoporous structures and a narrow distribution of pore sizes.[63] The inset of Figure 2b depicts the pore size distribution of 1DHS TiO_2, calculated by the Barrett–Joyner–Halenda method from the two branches of the isotherm. The 1DHS TiO_2 has a narrow distribution of pore diameters centered at 7 and 9 nm from the desorption and adsorption branches, respectively, roughly matching the dimension of GOx molecules (7.0 nm × 5.5 nm ×8.0 nm).[64] The 1DHS TiO_2 was also estimated to have a specific surface area as high as 218.4 $m^2\ g^{-1}$, as analyzed by the Brunauer–Emmett–Teller (BET) method.

Immobilization of GOx on 1DHS TiO_2. To find the optimal immobilization concentration of GOx on 1DHS TiO_2, we investigated the nitrogen adsorption–desorption isotherms of 1DHS TiO_2 before and after GOx loading with different initial concentrations of GOx. Since increases in the GOx concentration resulted in decreases in both the pore diameter and the pore volume (Table S1, Supporting Infomation), we can infer that the GOx, when introduced, fills in the pores of the 1DHS TiO_2. As a result, the hysteresis loop shows that the amount of adsorbed nitrogen decreases as the GOx loading increases (Figure 3). The inset of Figure 3 depicts the relationship between the initial GOx concentration and the final weight of GOx loaded on the TiO_2 material. Increases in the GOx concentration lead to increases in the amount of protein immobilized on the TiO_2, reaching a maximum loading of 42.7% at the GOx concentration of 10 mg mL^{-1}. Further increases in the GOx concentration do not result in increases in the protein loading, most likely due to the complete filling of pore spaces in 1DHS TiO_2. A quantity of 10 mg mL^{-1} of GOx was therefore used for protein immobilization in the later experiment.

The effectiveness of protein immobilization on 1DHS TiO_2 was investigated by IR spectroscopy (Figure 4) to detect the conformational changes of the secondary structure of the proteins. The spectrum of pure GOx molecules exhibits two characteristic peaks at 1658 and 1545 cm^{-1}, corresponding to the typical amide I and amide II adsorption bands of proteins.[23] The signal peaking at 1103 cm^{-1} is attributed to the C−O bond stretching vibration of GOx.[29] The 1DHS TiO_2 has bands at 1635 and 1040 cm^{-1}, which are ascribed to the deformational vibration of the H−O−H bond from absorbed water and the stretching vibration of the Ti−O−C bond from the hydrolysis of TIP, respectively.[25] The amide adsorption peaks are generally used as an indication of protein denaturation and conformational change upon immobilization. The presence of both amide I and II adsorption peaks in the spectrum of GOx-loaded 1DHS TiO_2 indicates that the enzyme retained its secondary structure after being adsorbed on the surface of TiO_2. The biocompatible nature of 1DHS TiO_2 may allow GOx to maintain its native structure, thus preventing denaturation of GOx. The amide adsorption peaks are downshifted slightly to 1647 and 1533 cm^{-1}, possibly due to the strong electrostatic interaction between the anchored enzyme and the TiO_2 (GOx is negatively charged in a neutral solution [isoelectric point (pI) = 4.2],[65] while TiO_2 is positively charged in a neutral solution due to its relatively high pI).[66] In addition, a downshift of the Ti−O−C adsorption peak is observed in the spectrum of GOx-loaded 1DHS TiO_2, further corroborating the electrostatic interaction between the negatively charged GOx and the positively charged TiO_2. The surface density of GOx on the electrode is calculated to be 83.4% by electrochemical impedance spectroscopy (EIS), which is an efficient method to investigate the surface properties of biomolecule-modified electrodes (Figure S3, Supporting Infomation).

Direct Electrochemistry of GOx Immobilized on 1DHS TiO_2. To study the direct electron transfer of GOx immobilized on 1DHS TiO_2, cyclic voltammetry (CV) measurements were performed using 1DHS TiO_2/Nafion-, GOx/Nafion-, and GOx/1DHS TiO_2/Nafion-modified GCEs in 0.1 M nitrogen-saturated phosphate-buffered saline (PBS) solution (pH = 7.4) at a scan rate of 100 mV s^{-1}. A high scanning rate in CV measurement is used to achieve reversibility of an electrochemical reaction.[25] As shown in Figure 5, TiO_2/Nafion- and GOx/Nafion-modified electrodes exhibited only typical square-shaped CV curves as a result of double-layer capacitance in the applied potential window, indicating that both the 1DHS TiO_2 and GOx are electrochemically inactive over this potential range. In contrast, two well-defined redox peaks are observed in the CV of the GOx/1DHS TiO_2/Nafion-modified GCE, with a cathodic peak potential (E_{pc}) of −0.481 V and an anodic peak potential (E_{pa}) of −0.443 V. The formal potential (E^0) of 0.462 V

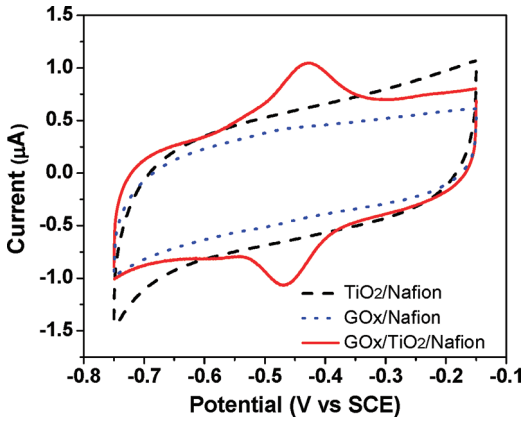

Figure 5. CVs of 1DHS TiO_2/Nafion-, GOx/Nafion-, and GOx/1DHS TiO_2/Nafion-modified GCEs measured in 0.1 M nitrogen-saturated PBS solution (pH = 7.4) at scan rate of 100 mV s^{-1}.

in our study conforms well to the standard electrode potential of FAD/$FADH_2$ in a neural solution,[25,29] indicating that the redox center of GOx immobilized on the 1DHS TiO_2 undergoes a quasi-reversible reaction on the electrode during the CV cycle:

$$GOx(FAD) + 2H^+ + 2e^- \rightarrow GOx(FADH_2) \quad (1)$$

$$GOx(FADH_2) - 2e^- \rightarrow GOx(FAD) + 2H^+ \quad (2)$$

where FAD and $FADH_2$ are the oxidized and reduced forms of the GOx redox center, respectively. This result illustrates that the 1DHS TiO_2 is apparently capable of mediating protein DET on the electrode. The heterogeneous electron-transfer rate constant k_s of GOx immobilized on 1DHS TiO_2 is calculated to be 7.8 s^{-1} according to Laviron's model,[67] a value that is substantially greater than that of GOx immobilized on other materials, *e.g.*, porous TiO_2 (3.96 s^{-1}),[25] NiO (3.12 s^{-1}),[29] MWCNTs (1.53 s^{-1})[68] and SWCNTs (0.3 s^{-1}).[69] This remarkably improved electrochemical response of GOx on 1DHS TiO_2 could be attributed to several factors. First, the GOx could enter the pores in the 1DHS TiO_2 due to the similarity in their sizes, providing omnidirectional contacts to the TiO_2 surface and significantly shortening the electron tunneling distance between the enzyme's active center and the material's conductive site. Second, the strong electrostatic interaction between GOx and TiO_2 could further narrow the spacing between the material and the adsorbed protein, thereby facilitating electron transfer between the electrode and immobilized GOx molecules. Finally, the high conductivity and low charge transfer resistance of 1DHS TiO_2 could provide a conduction pathway for electron-transfer, which is also favorable for the direct electrochemical reaction of immobilized proteins.

The electroactive protein density (Γ, mol cm^{-2}) of the GOx/1DHS TiO_2/Nafion-modified electrode could

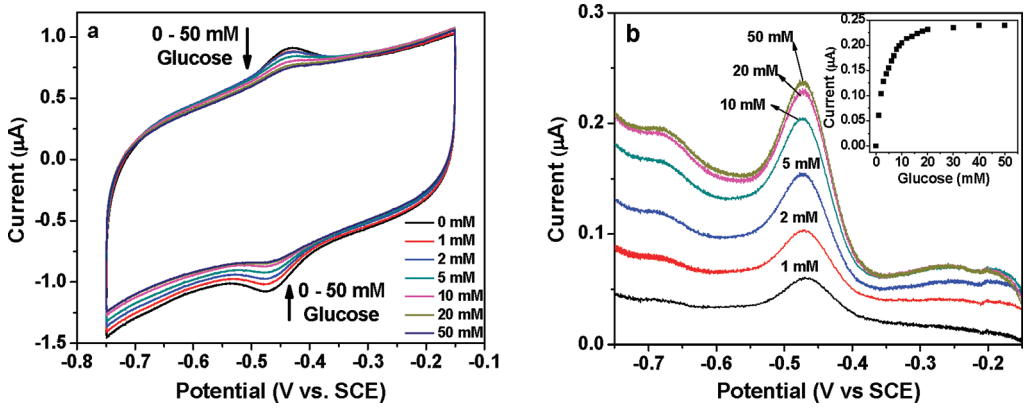

Figure 6. (a) CVs of a GOx/1DHS TiO_2/Nafion-modified GCE in 0.1 M of nitrogen-saturated PBS solution (pH = 7.4) with different glucose concentrations (some data not shown for clarity). (b) Cathodic branches of the background-subtracted CV curves in (a). Inset of (b) is the calibration curve. Scan rate: 100 mV s^{-1}.

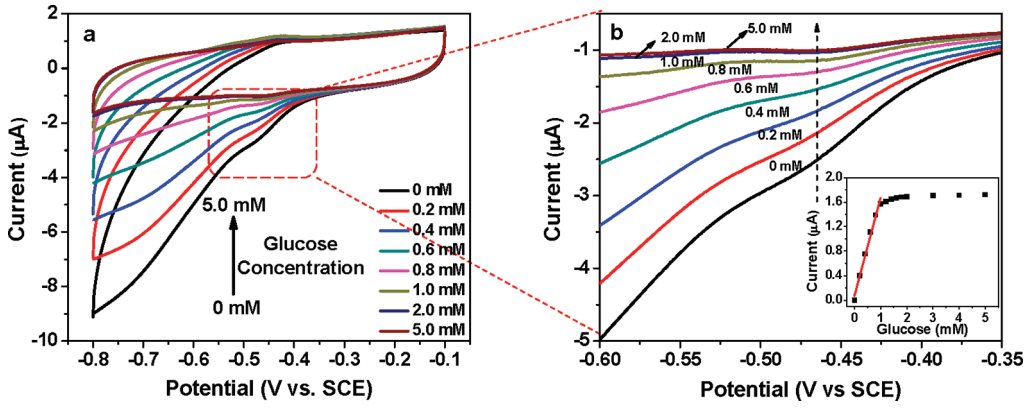

Figure 7. (a) CVs of a GOx/1DHS TiO_2/Nafion-modified GCE in 0.1 M of air-saturated PBS solution with (pH = 7.4) different glucose concentrations (some data not shown for clarity). (b) Enlarged graph showing the rectangular region marked in (a). Inset of (b): The calibration plot of the cathodic current *versus* the glucose concentration at −0.462 V. Scan rate: 100 mV s^{-1}.

be estimated from the integration of the reduction peak at 100 mV s^{-1} by the following equation:

$$Q = nFA\Gamma \quad (3)$$

Where Q is the total charge passing through the electrode, n is the number of electrons being transferred, F is Faraday's constant, and A is the geometric area of the electrode's surface. The surface coverage of electroactive GOx is calculated to be 6.86×10^{-10} mol cm^{-2}, a value that is much greater than that observed for GOx immobilized on porous TiO_2 (2.57×10^{-10} mol cm^{-2}),[25] PEDOT-NiO NS (1.56×10^{-10} mol cm^{-2}),[29] AuNPs (9.8×10^{-12} mol cm^{-2}),[70] and CdS (1.54×10^{-11} mol cm^{-2}).[71] The measured GOx loading of 42.7% and the surface GOx coverage of 83.4% can be converted to a surface adsorption density of 1.82×10^{-9} mol cm^{-2} by taking account of the dimension of GOx (7.0 ×5.5 ×8.0 nm) and specific surface area of 1DHS TiO_2 (218.4 m^2 g^{-1}). We can infer that approximately 37.7% of the enzyme immobilized on the 1DHS TiO_2 retains its electroactivity and achieves direct electrochemistry on the modified electrode surface. The results further corroborate that the 1DHS TiO_2 material has great biocompatibility that could well maintain the native structure of absorbed GOx, as confirmed by the FTIR results.

The electrochemical response of GOx immobilized on the 1DHS TiO_2 also displays strong dependence on the scanning rate (Figure S4, Supporting Infomation) and solution pH value (Figure S5, Supporting Infomation), showing that the redox reaction of FAD/$FADH_2$ in the active center of GOx is a surface-confined reaction and a two-electron coupled electrochemical process. The proposed mechanisms are specifically described in the Supporting Information.

Glucose Oxidation and Oxygen Reduction on GOx/1DHS TiO_2. To study glucose oxidation through the direct electrochemical reaction of GOx on 1DHS TiO_2, CV measurements of the GOx/1DHS TiO_2/Nafion-modified electrode were carried out in a nitrogen-saturated PBS solution containing different concentrations of glucose (0, 1, 2, 5, 10, 20, and 50 mM glucose) (Figure 6a). A pair of well-defined redox peaks is observed in the absence of glucose due to the reversible reaction of FAD/$FADH_2$. With increases in the glucose concentration, both the anodic and cathodic peak currents decrease, which

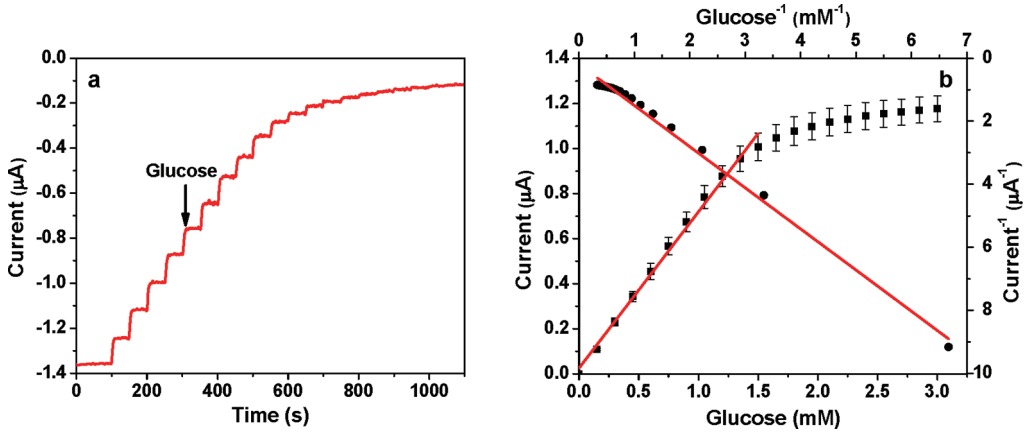

Figure 8. (a) Current−time curve of a GOx/1DHS TiO_2/Nafion-modified GCE for successive addition of 0.15 mM of glucose aliquots to stirred 0.1 M of air-saturated PBS (pH = 7.4) at −0.45 V. (b) The calibration curve (current *versus* glucose concentration) and the Lineweaver−Burk plot (current^{-1} *versus* concentration^{-1}) obtained from the amperometric response in (a).

could be explained by the following reaction:

$$\text{glucose} + \text{GOx(FAD)} \rightarrow \text{gluconicacid} + \text{GOx(FADH}_2\text{)} \quad (4)$$

The equation indicates that FAD at the redox center of GOx is directly involved in the glucose oxidation reaction. As glucose concentration increases, GOx(FAD) is increasingly converted into GOx($FADH_2$), leading to a continuous decrease in the cathodic and corresponding anodic peak currents. Figure 6b depicts the cathodic branches of the background-subtracted CV curves in Figure 6a (Figure 6a was converted to the current increase by subtracting the background CV curve (0 mM glucose) from other CV curves (1−50 mM glucose)). The cathodic current increases linearly with the glucose concentration up to 10 mM (inset of Figure 6b). This result indicates that the direct electrochemical reaction of protein achieved on the electrode could be effectively employed for glucose sensing without any mediator. The sensing mechanism in our system is different from those of both first-generation glucose sensors, in which glucose oxidation is based on oxygen reduction, and second-generation glucose sensors, which require a mediator to transfer the electrons between GOx and electrode.[11]

Similar CV measurements were conducted in air-saturated PBS solution containing different glucose concentrations on the GOx/1DHS TiO_2/Nafion-modified electrode. In contrast to the curves obtained in nitrogen-saturated PBS, a huge cathodic current is observed in the CV cycle at a potential of less than −0.4 V in the absence of glucose (Figure 7a), arising from the electrocatalytic reduction of the dissolved oxygen by the GOx/1DHS TiO_2/Nafion-modified electrode.[29,70] However, the reductive current at the FAD redox potential gradually decreases with increases in the glucose concentration, exhibiting a linear relationship with the glucose concentration in the range of 0.2−1.0 mM. The current starts to saturate at 1.0 mM of glucose and quickly reaches a maximum at 2.0 mM (Figure 7b). The relatively smaller linear range, however, is compensated by the remarkably enhanced sensitivity, which is nearly 40 times higher than the corresponding value measured in nitrogen-saturated PBS, possibly due to the integral effect of FAD reduction by glucose (eq 4) and competitive oxygen consumption by both glucose and $FADH_2$ (eqs 5 and 6).[29]

TABLE 1. Comparison of the Analytical Performance of Metal Oxide-Based Glucose Sensors.

electrode material	sensitivity (μA mM^{-1} cm^{-2})	response time (s)	ref
GOx/1DHS TiO_2	9.9	<5	this work
GOx/mesoporous TiO_2	3.9	<10	25
GOx/nanocrystalline TiO_2	4.6	<30	76
GOx/TiO_2-copolymer	2.3	<20	77
GOx/porous carbon-silica	1.8	~4	23
GOx/NiO hollow spheres	3.4	~8	78

$$\text{glucose} + O_2 \rightarrow \text{gluconicacid} + H_2O_2 \quad (5)$$

$$\text{GOx(FADH}_2\text{)} + O_2 \rightarrow \text{GOx(FAD)} + H_2O_2 \quad (6)$$

Glucose Sensing Performance of the GOx/1DHS TiO_2/Nafion-Modified Electrode. The glucose sensing performance of the GOx/1DHS TiO_2/Nafion-modified electrode was evaluated by amperometric measurements in air-saturated PBS at a fixed potential of −0.45 V, where a decrease in the voltammetric currents is observed with the repeated addition of glucose. Figure 8a shows the typical amperogram obtained by successive additions of 0.15 mM (2.25 μmol) of glucose into homogeneously stirred 0.1 M of PBS (pH of 7.4) with a time interval of 50 s. Each injection of 0.15 mM of glucose results in a decrease of 120 nA in the cathodic current for the first 10 steps, which gives rise to a sensitivity of 9.90 μA mM^{-1} cm^{-2}. In addition, 95% of

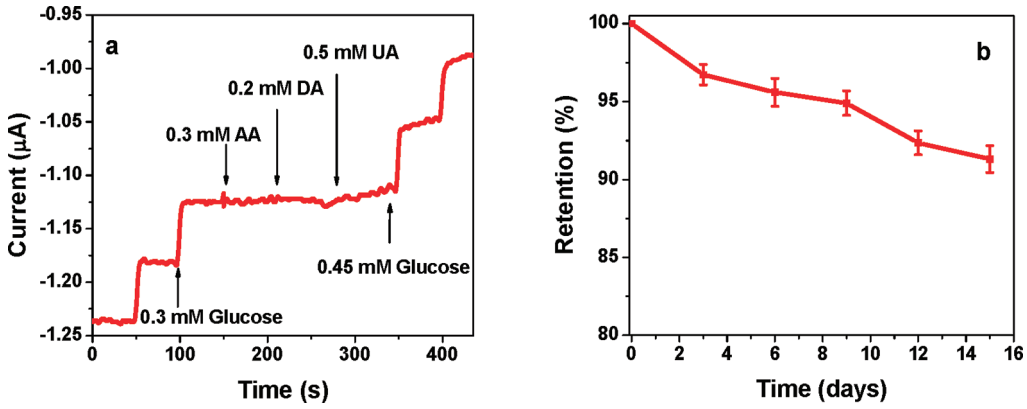

Figure 9. (a) Amperogram showing the effect of interfering compounds (0.3 mM of AA, 0.2 mM of DA, and 0.5 mM of UA) on the detection of glucose. (b) The stability of the GOx/1DHS TiO_2/Nafion-modified electrode over a two-week storage period.

the steady-state current could be reached within 5 s upon the addition of glucose, reflecting the fast response of our glucose sensor. Both the sensitivity and the response time of our sensor are greatly superior to those of other metal oxide-based glucose biosensors, which are listed in Table 1. Figure 8b depicts the calibration curve of the modified electrode obtained from the current–time plot, showing a well-defined typical behavior of an enzymatic reaction with a linear range up to 1.5 mM. A current plateau is observed when the glucose concentration is higher than 1.5 mM. A linear regression equation of $I(\mu A) = 0.80(\mu A\ mM^{-1}) \times C\ (mM)$, ($n = 3$, $R = 0.994$) is thus derived from the calibration curve, revealing that the glucose sensor has a detection limit as low as 1.29 μM ($S/N = 3$). The apparent Michaelis–Menten constant K_m^{app} is calculated using the electrochemical version of the Lineweaver–Burk equation:[72]

$$\frac{1}{i_{ss}} = \frac{K_m^{app}}{i_{max}}\frac{1}{C} + \frac{1}{i_{max}} \qquad (7)$$

where i_{ss} is the steady-state current, i_{max} is the saturation current, and C is the glucose concentration. K_m^{app} is determined to be 1.54 mM from the intercept and slope of the Lineweaver–Burk plot (Figure 8b), a value that is much lower than the value of 8.5 mM for GOx immobilized on carbon nanohorns[73] and 6.08 mM for GOx immobilized on redox polymers.[74] The smaller K_m^{app} indicates that the GOx/1DHS TiO_2-modified electrode has superior enzymatic activity and higher affinity for the glucose substrate.[29]

The GOx/1DHS TiO_2-modified electrode also exhibits excellent selectivity for glucose detection. As shown in Figure 9a, the addition of interferents, *e.g.*, 0.3 mM of ascorbic acid (AA), 0.2 mM of dopamine (DA) and 0.5 mM of uric acid (UA), in 0.1 M PBS containing 0.6 mM of glucose gives rise to negligible current changes, while a significant current response is observed for the subsequent addition of 0.45 mM of glucose. To assess its stability, the GOx/1DHS TiO_2-modified electrode was stored at 4 °C after use and used to measure the current response for 0.3 mM of glucose every three days. The GOx/1DHS TiO_2/Nafion-modified electrode retains 91.2% of its original current response over a storage period of 2 weeks (Figure 9b), indicating a good shelf lifetime for the modified electrode. In addition, upon repeated scanning of the GOx/1DHS TiO_2-modified electrode in 0.1 M of PBS containing 0.3 mM of glucose at 100 mV s^{-1}, the voltammetric current response was observed to decrease very slowly, *i.e.*, a peak current drop of 4.5%, even after continuous sweeping for 5 h. Moreover, UV–vis spectroscopy reveals no desorbed GOx detectable in the CV measurement solution, possibly due to the protein-leaching barrier formed by the Nafion membrane on the electrode. The superior sensing performance and long-term storage stability of the GOx/1DHS TiO_2-modified electrode may be attributable to the unique structure and great biocompatibility of 1DHS TiO_2 and to the strong electrostatic interaction between GOx and the synthesized TiO_2 material.

CONCLUSION

In the present work, a novel material, 1DHS TiO_2, was synthesized, characterized, and used for the immobilization of GOx for direct electrochemical reactions and mediator-free glucose sensing. The 1DHS TiO_2 was easily synthesized by a solvothermal method using MWCNT as a template with a large surface area and a narrow pore size distribution. The protein immobilization was characterized by BET, FTIR, and EIS, revealing that GOx immobilized on 1DHS TiO_2 maintained its original conformation well and that the maximum protein loading on 1DHS TiO_2 was achieved at a GOx concentration of 10 mg mL^{-1}. The great biocompatibility of 1DHS TiO_2 and the electrostatic interaction between GOx and 1DHS TiO_2 may contribute to the high bioactivity of the immobilized proteins. The electrochemical properties of GOx immobilized on 1DHS TiO_2 were studied systematically. These electrochemical properties included fast direct electrochemical reactions, surface-confined electron-transfer behavior, and strong pH dependence. The sensing mechanism of protein DET on 1DHS TiO_2 was demonstrated by cyclic

voltammetry in both nitrogen-saturated PBS and air-saturated PBS. The experimental data revealed that the combined effect of glucose oxidation by FAD and oxygen reduction by both glucose and $FADH_2$ resulted in a significant decrease in the cathodic current and allowed for a high sensitivity for glucose detection. The analytical performance of the GOx/1DHS TiO_2/Nafion-modified electrode was investigated by the amperometric response, showing a fast response, good specificity, and long-term stability. Our study not only demonstrates a unique structured and biocompatible TiO_2 nanomaterial suitable for protein immobilization, direct electrochemical reactions, and the construction of third-generation biosensors but also provides fundamental insights leading to the understanding of the mechanism of protein DET on nanomaterials, especially the direct electrochemical reaction of GOx for glucose sensing.

EXPERIMENTAL SECTION

Chemicals and Materials. Glucose, glucose oxidase from *Aspergillus niger* (GOx, 100 000−250 000 units/g), diethylenetriamine (DETA; 99%), and titanium(IV) isopropoxide (TIP; 97%) were obtained from Sigma-Aldrich. MWCNTs were purchased from X2 Labwares. All other chemicals were of analytical grade, and all solutions were prepared in double-distilled water.

Synthesis of 1DHS TiO_2. The CNT-TiO_2 composite was synthesized using our previous method.[75] Briefly, 50 mg of acid-treated MWCNTs was dispersed in 40 mL of isopropyl alcohol (IPA) by sonication for 10 min, followed by the addition of 0.03 mL of DETA. After gentle stirring for 2 min, 1.8 mL of TIP was added. The solution was then transferred into a 60 mL Teflon-lined stainless steel autoclave and kept in an electric oven at 200 °C for 24 h. The autoclave was then taken out of the oven and left to cool down to room temperature. The black precipitate was collected by centrifugation, washed thoroughly with ethanol, and dried at 60 °C overnight. To obtain the 1DHS TiO_2, the as-prepared composite was subjected to calcination at 550 °C for 2 h to remove the MWCNT template and obtain the hierarchically structured 1D TiO_2.

Protein Immobilization and Electrode Preparation. Protein immobilization was achieved by immersing 10 mg of the synthesized TiO_2 material in 1 mL of GOx solution (10 mg mL^{-1}) prepared in 0.1 M of PBS (pH = 7.4) under ambient conditions, followed by vigorously shaking of the solution for 0.5 h. The solution was then stored at 4 °C overnight to allow protein adsorption. The concentrations of GOx in the solution before and after protein adsorption were determined by UV−vis spectroscopy at 280 nm. The GOx loading on 1DHS TiO_2 was calculated by subtracting the amount of the remaining GOx in supernatant solution after adsorption from the initial amount of GOx. The bioconjugate obtained was later subjected to centrifugation, and the pellet was dispersed in 1 mL of protein-free PBS solution by continuously shaking the mixture for 0.5 h. For Fourier transform infrared (FT-IR) measurement, the obtained pellet was then subjected to washing with PBS for three times and drying in vacuum. The dried samples were pressed into pellets together with potassium bromide (KBr) for FT-IR spectroscopy by Bruker EQUINOX 55 Duroscope. A glassy carbon electrode (GCE, 3 mm in diameter) was polished to a mirror-like surface with 1.0, 0.3, and 0.05 μm alumina powder, followed by sonication in acetone, ethanol, and water for 3 min, respectively. Then the electrode was thoroughly rinsed with double-distilled water and dried using ultrapure nitrogen. Electrode modification was achieved by depositing 5 μL of the reshaken bioconjugate dispersion on the center of the precleaned GCE, which was left to dry at 4 °C overnight. Finally, 10 μL of 0.5% Nafion was dropped on the whole electrode surface to fix the modifier on the electrode.

Apparatus. The product morphology was examined using FESEM (JEOL, JSM-6700F, 5 kV) and TEM (JEOL, JEM-2100F, 200 kV). Crystallographic information for the samples was collected using XRD (Bruker, D8 Advance X-ray diffractometer, Cu Kα, λ = 1.5406 Å). The specific surface area and pore size distribution of the products were measured using a BET analyzer (Quantachrome Instruments, Autosorb AS-6B) at 77 K. Protein immobilization was investigated by FTIR (Bruker EQUINOX 55 DuroscopeTM). The UV spectra were recorded with Shimadzu UV-3600 UV−vis spectrophotometer (Japan).

All electrochemical measurements were carried out using a CHI 660C electrochemical workstation (CH Instrument, USA) with a conventional three-electrode system, which employed a GCE as the working electrode, a platinum wire as the counter electrode, and a saturated calomel electrode (SCE) as the reference electrode. CV studies were performed in deoxygenated PBS solution unless otherwise specified. Ultrapure nitrogen was bubbled through the PBS solution for 10 min before the experiment, and the solution was maintained under a nitrogen atmosphere during the measurement. Electrochemical impedance spectroscopy (EIS) measurements were conducted in a 1.0 M of KCl solution containing 10 mM of $Fe(CN)_6^{3-/4-}$.

Acknowledgment. We gratefully acknowledge the Nanyang Technological University for support of this work. We are also grateful for the financial support from the Academic Research Funding Tier 1 (RG65/08).

Supporting Information Available: SEM, TEM, EDX, EIS, and additional electrochemical performance figures. This material is available free of charge *via* the Internet at http://pubs.acs.org.

REFERENCES AND NOTES

1. Beissenhirtz, M. K.; Scheller, F. W.; Stocklein, W. F. M.; Kurth, D. G.; Mohwald, H.; Lisdat, F. Electroactive Cytochrome C Multilayers within a Polyelectrolyte Assembly. *Angew Chem. Int. Ed.* **2004**, *43*, 4357–4360.
2. El Kasmi, A.; Wallace, J. M.; Bowden, E. F.; Binet, S. M.; Linderman, R. J. Controlling Interfacial Electron-Transfer Kinetics of Cytochrome C with Mixed Self-Assembled Monolayers. *J. Am. Chem. Soc.* **1998**, *120*, 225–226.
3. Wei, J. J.; Liu, H. Y.; Dick, A. R.; Yamamoto, H.; He, Y. F.; Waldeck, D. H. Direct Wiring of Cytochrome C's Heme Unit to an Electrode: Electrochemical Studies. *J. Am. Chem. Soc.* **2002**, *124*, 9591–9599.
4. Deng, S. Y.; Jian, G. Q.; Lei, J. P.; Hu, Z.; Ju, H. X. A Glucose Biosensor Based on Direct Electrochemistry of Glucose Oxidase Immobilized on Nitrogen-Doped Carbon Nanotubes. *Biosens. Bioelectron.* **2009**, *25*, 373–377.
5. Shan, C. S.; Yang, H. F.; Song, J. F.; Han, D. X.; Ivaska, A.; Niu, L. Direct Electrochemistry of Glucose Oxidase and Biosensing for Glucose Based on Graphene. *Anal. Chem.* **2009**, *81*, 2378–2382.
6. Xiao, Y.; Patolsky, F.; Katz, E.; Hainfeld, J. F.; Willner, I. "Plugging into Enzymes": Nanowiring of Redox Enzymes by a Gold Nanoparticle. *Science* **2003**, *299*, 1877–1881.
7. Chaudhuri, S. K.; Lovley, D. R. Electricity Generation by Direct Oxidation of Glucose in Mediatorless Microbial Fuel Cells. *Nat. Biotechnol.* **2003**, *21*, 1229–1232.
8. Ivnitski, D.; Branch, B.; Atanassov, P.; Apblett, C. Glucose Oxidase Anode for Biofuel Cell Based on Direct Electron Transfer. *Electrochem. Commun.* **2006**, *8*, 1204–1210.
9. Yan, Y. M.; Zheng, W.; Su, L.; Mao, L. Q. Carbon-Nanotube-Based Glucose/O2 Biofuel Cells. *Adv. Mater.* **2006**, *18*, 2639–2643.
10. Riklin, A.; Katz, E.; Willner, I.; Stocker, A.; Buckmann, A. F. Improving Enzyme-Electrode Contacts by Redox Modification of Cofactors. *Nature* **1995**, *376*, 672–675.

11. Ronkainen, N. J.; Halsall, H. B.; Heineman, W. R. Electrochemical Biosensors. *Chem. Soc. Rev.* **2010**, *39*, 1747–1763.
12. Wang, J. Glucose Biosensors: 40 Years of Advances and Challenges. *Electroanalysis* **2001**, *13*, 983–988.
13. Wang, J. Electrochemical Glucose Biosensors. *Chem. Rev.* **2008**, *108*, 814–825.
14. Si, P.; Kannan, P.; Guo, L.; Son, H.; Kim, D.-H. Highly Stable and Sensitive Glucose Biosensor Based on Covalently Assembled High Density Au Nanostructures. *Biosens. Bioelectron.* **2011**, *26*, 3845–3851.
15. Kandimalla, V. B.; Tripathi, V. S.; Ju, H. X. A Conductive Ormosil Encapsulated with Ferrocene Conjugate and Multiwall Carbon Nanotubes for Biosensing Application. *Biomaterials* **2006**, *27*, 1167–1174.
16. Ivnitski, D.; Artyushkova, K.; Rincon, R. A.; Atanassov, P.; Luckarift, H. R.; Johnson, G. R. Entrapment of Enzymes and Carbon Nanotubes in Biologically Synthesized Silica: Glucose Oxidase-Catalyzed Direct Electron Transfer. *Small* **2008**, *4*, 357–364.
17. Guo, L.; Ferhan, A. R.; Lee, K.; Kim, D.-H. Nanoarray-Based Biomolecular Detection Using Individual Au Nanoparticles with Minimized Localized Surface Plasmon Resonance Variations. *Anal. Chem.* **2011**, *83*, 2605–2612.
18. Qiao, S. Z.; Zhang, L.; Geng, W. C.; Zheng, H. J.; Lu, G. Q.; Yan, Z. F. Fabrication and Biosensing with Cnt/Aligned Mesostructured Silica Core-Shell Nanowires. *ACS Appl. Mater. Interfaces* **2010**, *2*, 2767–2772.
19. Liu, A.; Wei, M.; Honma, I.; Zhou, H. Direct Electrochemistry of Myoglobin in Titanate Nanotubes Film. *Anal. Chem.* **2005**, *77*, 8068–8074.
20. McKenzie, K. J.; Marken, F. Accumulation and Reactivity of the Redox Protein Cytochrome C in Mesoporous Films of TiO_2 Phytate. *Langmuir* **2003**, *19*, 4327–4331.
21. Liu, G. Z.; Paddon-Row, M. N.; Gooding, J. J. A Molecular Wire Modified Glassy Carbon Electrode for Achieving Direct Electron Transfer to Native Glucose Oxidase. *Electrochem. Commun.* **2007**, *9*, 2218–2223.
22. Zhang, J.; Feng, M.; Tachikawa, H. Layer-by-Layer Fabrication and Direct Electrochemistry of Glucose Oxidase on Single Wall Carbon Nanotubes. *Biosens. Bioelectron.* **2007**, *22*, 3036–3041.
23. Wu, S.; Ju, H. X.; Liu, Y. Conductive Mesocellular Silica-Carbon Nanocomposite Foams for Immobilization, Direct Electrochemistry, and Biosensing of Proteins. *Adv. Funct. Mater.* **2007**, *17*, 585–592.
24. Gooding, J. J.; Wibowo, R.; Liu, J. Q.; Yang, W. R.; Losic, D.; Orbons, S.; Mearns, F. J.; Shapter, J. G.; Hibbert, D. B. Protein Electrochemistry Using Aligned Carbon Nanotube Arrays. *J. Am. Chem. Soc.* **2003**, *125*, 9006–9007.
25. Bao, S. J.; Li, C. M.; Zang, J. F.; Cui, X. Q.; Qiao, Y.; Guo, J. New Nanostructured Tio2 for Direct Electrochemistry and Glucose Sensor Applications. *Adv. Funct. Mater.* **2008**, *18*, 591–599.
26. Peng, H. P.; Liang, R. P.; Qiu, J. D. Facile Synthesis of Fe3O4@Al2O3 Core-Shell Nanoparticles and Their Application to the Highly Specific Capture of Heme Proteins for Direct Electrochemistry. *Biosens. Bioelectron.* **2011**, *26*, 3005–3011.
27. Zhu, Z. H.; Qu, L. N.; Niu, Q. J.; Zeng, Y.; Sun, W.; Huang, X. T. Urchinlike MnO2 Nanoparticles for the Direct Electrochemistry of Hemoglobin with Carbon Ionic Liquid Electrode. *Biosens. Bioelectron.* **2011**, *26*, 2119–2124.
28. Wang, Z. Y.; Liu, S. N.; Wu, P.; Cai, C. X. Detection of Glucose Based on Direct Electron Transfer Reaction of Glucose Oxidase Immobilized on Highly Ordered Polyaniline Nanotubes. *Anal. Chem.* **2009**, *81*, 1638–1645.
29. Guo, C. X.; Li, C. M. Direct Electron Transfer of Glucose Oxidase and Biosensing of Glucose on Hollow Sphere-Nanostructured Conducting Polymer/Metal Oxide Composite. *Phys. Chem. Chem. Phys.* **2010**, *12*, 12153–12159.
30. Bach, U.; Lupo, D.; Comte, P.; Moser, J. E.; Weissortel, F.; Salbeck, J.; Spreitzer, H.; Gratzel, M. Solid-State Dye-Sensitized Mesoporous Tio2 Solar Cells with High Photon-to-Electron Conversion Efficiencies. *Nature* **1998**, *395*, 583–585.
31. Oregan, B.; Gratzel, M.; Low-Cost, A High-Efficiency Solar-Cell Based on Dye-Sensitized Colloidal TiO_2 Films. *Nature* **1991**, *353*, 737–740.
32. Fujishima, A.; Honda, K. Electrochemical Photolysis of Water at a Semiconductor Electrode. *Nature* **1972**, *238*, 37–38.
33. Mor, G. K.; Shankar, K.; Paulose, M.; Varghese, O. K.; Grimes, C. A. Enhanced Photocleavage of Water Using Titania Nanotube Arrays. *Nano Lett.* **2005**, *5*, 191–195.
34. Gratzel, M. Materials Science - Ultrafast Colour Displays. *Nature* **2001**, *409*, 575–576.
35. Hagfeldt, A.; Gratzel, M. Light-Induced Redox Reactions in Nanocrystalline Systems. *Chem. Rev.* **1995**, *95*, 49–68.
36. Chen, J. S.; Tan, Y. L.; Li, C. M.; Cheah, Y. L.; Luan, D.; Madhavi, S.; Boey, F. Y. C.; Archer, L. A.; Lou, X. W. Constructing Hierarchical Spheres from Large Ultrathin Anatase TiO_2 Nanosheets with Nearly 100% Exposed (001) Facets for Fast Reversible Lithium Storage. *J. Am. Chem. Soc.* **2010**, *132*, 6124–6130.
37. Ding, S. J.; Chen, J. S.; Luan, D. Y.; Boey, F. Y. C.; Madhavi, S.; Lou, X. W. Graphene-Supported Anatase TiO_2 Nanosheets for Fast Lithium Storage. *Chem. Commun.* **2011**, *47*, 5780–5782.
38. Varghese, O. K.; Gong, D. W.; Paulose, M.; Ong, K. G.; Dickey, E. C.; Grimes, C. A. Extreme Changes in the Electrical Resistance of Titania Nanotubes with Hydrogen Exposure. *Adv. Mater.* **2003**, *15*, 624–627.
39. Grimes, C. A.; Ong, K. G.; Varghese, O. K.; Yang, X. P.; Mor, G.; Paulose, M.; Dickey, E. C.; Ruan, C. M.; Pishko, M. V.; Kendig, J. W.; Mason, A. J. A Sentinel Sensor Network for Hydrogen Sensing. *Sensors* **2003**, *3*, 69–82.
40. Miyazaki, H.; Hyodo, T.; Shimizu, Y.; Egashira, M. Hydrogen-Sensing Properties of Anodically Oxidized Tio2 Film Sensors - Effects of Preparation and Pretreatment Conditions. *Sens. Actuators, B* **2005**, *108*, 467–472.
41. Liu, S. Q.; Chen, A. C. Coadsorption of Horseradish Peroxidase with Thionine on Tio2: Nanotubes for Biosensing. *Langmuir* **2005**, *21*, 8409–8413.
42. Topoglidis, E.; Campbell, C. J.; Cass, A. E. G.; Durrant, J. R. Factors That Affect Protein Adsorption on Nanostructured Titania Films. A Novel Spectroelectrochemical Application to Sensing. *Langmuir* **2001**, *17*, 7899–7906.
43. Cao, H. M.; Zhu, Y. H.; Tang, L. H.; Yang, X. L.; Li, C. Z. A Glucose Biosensor Based on Immobilization of Glucose Oxidase into 3d Macroporous Tio2. *Electroanalysis* **2008**, *20*, 2223–2228.
44. Chen, X.; Mao, S. S. Titanium Dioxide Nanomaterials: Synthesis, Properties, Modifications, and Applications. *Chem. Rev.* **2007**, *107*, 2891–2959.
45. Burda, C.; Chen, X. B.; Narayanan, R.; El-Sayed, M. A. Chemistry and Properties of Nanocrystals of Different Shapes. *Chem. Rev.* **2005**, *105*, 1025–1102.
46. Murray, C. B.; Kagan, C. R.; Bawendi, M. G. Synthesis and Characterization of Monodisperse Nanocrystals and Close-Packed Nanocrystal Assemblies. *Annu. Rev. Mater. Sci.* **2000**, *30*, 545–610.
47. Hendren, W. R.; Murphy, A.; Evans, P.; O'Connor, D.; Wurtz, G. A.; Zayats, A. V.; Atkinson, R.; Pollard, R. J. Fabrication and Optical Properties of Gold Nanotube Arrays. *J. Phys.: Condens. Matter* **2008**, *20*, 362203.
48. Lee, H. O.; Kim, E. M.; Yu, H.; Jung, J. S.; Chae, W. S. Advanced Porous Gold Nanofibers for Highly Efficient and Stable Molecular Sensing Platforms. *Nanotechnology* **2009**, *20*, 325604.
49. Yamaguchi, I.; Watanabe, M.; Shinagawa, T.; Chigane, M.; Inaba, M.; Tasaka, A.; Izaki, M. Preparation of Core/Shell and Hollow Nanostructures of Cerium Oxide by Electrodeposition on a Polystyrene Sphere Template. *ACS Appl. Mater. Interfaces* **2009**, *1*, 1070–1075.
50. Xia, X. H.; Tu, J. P.; Zhang, J.; Xiang, J. Y.; Wang, X. L.; Zhao, X. B. Cobalt Oxide Ordered Bowl-Like Array Films Prepared by Electrodeposition through Monolayer Polystyrene Sphere Template and Electrochromic Properties. *ACS Appl. Mater. Interfaces* **2009**, *2*, 186–192.
51. Peng, T. Y.; Hasegawa, A.; Qiu, J. R.; Hirao, K. Fabrication of Titania Tubules with High Surface Area and Well-Developed

Mesostructural Walls by Surfactant-Mediated Templating Method. *Chem. Mater.* **2003**, *15*, 2011–2016.
52. Fan, H.; Xu, Q.; Guo, Y.; Cao, Y. Al_2O_3/Fe_2O_3 Mesoporous Composite Prepared with Activated Carbon Template in Supercritical Carbon Dioxide. *Ind. Eng. Chem. Res.* **2006**, *45*, 5009–5012.
53. Lei, Y.; Zhang, L. D.; Fan, J. C. Fabrication, Characterization and Raman Study of TiO_2 Nanowire Arrays Prepared by Anodic Oxidative Hydrolysis of TiC3. *Chem. Phys. Lett.* **2001**, *338*, 231–236.
54. Liu, S. Q.; Huang, K. L. Straightforward Fabrication of Highly Ordered TiO_2 Nanowire Arrays in Aam on Aluminum Substrate. *Sol. Energy Mater. Sol. Cells* **2005**, *85*, 125–131.
55. Kang, T. S.; Smith, A. P.; Taylor, B. E.; Durstock, M. F. Fabrication of Highly-Ordered TiO_2 Nanotube Arrays and Their Use in Dye-Sensitized Solar Cells. *Nano Lett.* **2009**, *9*, 601–606.
56. Lai, M.; Lim, J. H.; Mubeen, S.; Rheem, Y.; Mulchandani, A.; Deshusses, M. A.; Myung, N. V. Size-Controlled Electrochemical Synthesis and Properties of SnO_2 Nanotubes. *Nanotechnology* **2009**, *20*, 185602.
57. Lou, X. W.; Archer, L. A.; Yang, Z. Hollow Micro-/Nanostructures: Synthesis and Applications. *Adv. Mater.* **2008**, *20*, 3987–4019.
58. Ding, S.; Chen, J. S.; Qi, G.; Duan, X.; Wang, Z.; Giannelis, E. P.; Archer, L. A.; Lou, X. W. Formation of SnO_2 Hollow Nanospheres inside Mesoporous Silica Nanoreactors. *J. Am. Chem. Soc.* **2010**, *133*, 21–23.
59. Yang, P. D.; Zhao, D. Y.; Margolese, D. I.; Chmelka, B. F.; Stucky, G. D. Generalized Syntheses of Large-Pore Mesoporous Metal Oxides with Semicrystalline Frameworks. *Nature* **1998**, *396*, 152–155.
60. Lee, J.; Yoon, S.; Oh, S. M.; Shin, C. H.; Hyeon, T. Development of a New Mesoporous Carbon Using an Hms Aluminosilicate Template. *Adv. Mater.* **2000**, *12*, 359–362.
61. Attard, G. S.; Glyde, J. C.; Goltner, C. G. Liquid-Crystalline Phases as Templates for the Synthesis of Mesoporous Silica. *Nature* **1995**, *378*, 366–368.
62. Zhao, D. Y.; Feng, J. L.; Huo, Q. S.; Melosh, N.; Fredrickson, G. H.; Chmelka, B. F.; Stucky, G. D. Triblock Copolymer Syntheses of Mesoporous Silica with Periodic 50 to 300 Angstrom Pores. *Science* **1998**, *279*, 548–552.
63. Kruk, M.; Jaroniec, M. Gas Adsorption Characterization of Ordered Organic-Inorganic Nanocomposite Materials. *Chem. Mater.* **2001**, *13*, 3169–3183.
64. Hartmann, M. Ordered Mesoporous Materials for Bioadsorption and Biocatalysis. *Chem. Mater.* **2005**, *17*, 4577–4593.
65. Pazur, J. H.; Kleppe, K. The Oxidation of Glucose and Related Compounds by Glucose Oxidase from Aspergillus Niger. *Biochemistry* **1964**, *3*, 578–583.
66. Solanki, P. R.; Malhotra, A. K. V. V. A.; Nanostructured Metal, B. D. Oxide-Based Biosensors. *NPG Asia Mater.* **2011**, 17–24.
67. Laviron, E. General Expression of the Linear Potential Sweep Voltammogram in the Case of Diffusionless Electrochemical Systems. *J. Electroanal. Chem.* **1979**, *101*, 19–28.
68. Cai, C. X.; Chen, J. Direct Electron Transfer of Glucose Oxidase Promoted by Carbon Nanotubes. *Anal. Biochem.* **2004**, *332*, 75–83.
69. Liu, J. Q.; Chou, A.; Rahmat, W.; Paddon-Row, M. N.; Gooding, J. J. Achieving Direct Electrical Connection to Glucose Oxidase Using Aligned Single Walled Carbon Nanotube Arrays. *Electroanalysis* **2005**, *17*, 38–46.
70. Liu, S. Q.; Ju, H. X. Reagentless Glucose Biosensor Based on Direct Electron Transfer of Glucose Oxidase Immobilized on Colloidal Gold Modified Carbon Paste Electrode. *Biosens. Bioelectron.* **2003**, *19*, 177–183.
71. Huang, Y. X.; Zhang, W. J.; Xiao, H.; Li, G. X. An Electrochemical Investigation of Glucose Oxidase at a Us Nanoparticles Modified Electrode. *Biosens. Bioelectron.* **2005**, *21*, 817–821.
72. Lineweaver, H.; Burk, D. The Determination of Enzyme Dissociation Constants. *J. Am. Chem. Soc.* **1934**, *56*, 658–666.
73. Xu, G. B.; Liu, X. Q.; Shi, L. H.; Niu, W. X.; Li, H. J. Amperometric Glucose Biosensor Based on Single-Walled Carbon Nanohorns. *Biosens. Bioelectron.* **2008**, *23*, 1887–1890.
74. Gregg, B. A.; Heller, A. Cross-Linked Redox Gels Containing Glucose-Oxidase for Amperometric Biosensor Applications. *Anal. Chem.* **1990**, *62*, 258–263.
75. Ding, S. J.; Chen, J. S.; Lou, X. W. One-Dimensional Hierarchical Structures Composed of Novel Metal Oxide Nanosheets on Carbon Nanotube Backbone and Their Lithium Storage Properties. *Adv. Funct. Mater* DOI: 10.1002/adfm.201100781.
76. Li, Q. W.; Luo, G. A.; Feng, J.; Zhou, Q.; Zhang, L.; Zhu, Y. F. Amperometric Detection of Glucose with Glucose Oxidase Absorbed on Porous Nanocrystalline TiO_2 Film. *Electroanalysis* **2001**, *13*, 413–416.
77. Chen, X.; Dong, S. J. Sol-Gel-Derived Titanium Oxide/Copolymer Composite Based Glucose Biosensor. *Biosens. Bioelectron.* **2003**, *18*, 999–1004.
78. Wang, T. H.; Li, C. C.; Liu, Y. L.; Li, L. M.; Du, Z. F.; Xu, S. J.; Zhang, M.; Yin, X. M.; Novel Amperometric, A Biosensor Based on NiO Hollow Nanospheres for Biosensing Glucose. *Talanta* **2008**, *77*, 455–459.